AST-2020-2345-ver9-Viennet_1P
Type: research-article

ASTROBIOLOGY
Volume 21, Number 7, 2021
© Mary Ann Liebert, Inc.
DOI: 10.1089/ast.2020.2345

Research Article

Martian Magmatic Clay Minerals Forming Vesicles: Perfect Niches for Emerging Life?

Jean-Christophe Viennet,[1] Sylvain Bernard,[1] Corentin Le Guillou,[2] Violaine Sautter,[1] Brian Grégoire,[3] Albert Jambon,[1] Sylvain Pont,[1] Olivier Beyssac,[1] Brigitte Zanda,[1] Roger Hewins,[1] and Laurent Remusat[1]

Abstract

Mars was habitable in its early history, but the consensus is that it is quite inhospitable today, in particular because its modern climate cannot support stable liquid water at the surface. Here, we report the presence of magmatic Fe/Mg clay minerals within the mesostasis of the martian meteorite NWA 5790, an unaltered 1.3 Ga nakhlite archetypal of the martian crust. These magmatic clay minerals exhibit a vesicular texture that forms a network of microcavities or pockets, which could serve as microreactors and allow molecular crowding, a necessary step for the emergence of life. Because their formation does not depend on climate, such niches for emerging life may have been generated on Mars at many periods throughout its history, regardless of the stability or availability of liquid water at the surface. Key Words: Mars—Clay minerals—Magmatism—Habitability—Meteorite. Astrobiology 21, xxx–xxx.

1. Introduction

The concept of habitability is essentially tied to the presence of liquid water at (or near) the surface of a planetary body. The surface of Mars was habitable during the Noachian (4.1–3.7 Ga) because liquid water was then both stable and available, at least episodically. Environments likely existed on Noachian Mars with liquid water and metabolic energy sources available for the development of life (Westall *et al.,* 2013; Grotzinger *et al.,* 2014; Kral *et al.,* 2014; Hurowitz *et al.,* 2017; McMahon *et al.,* 2018). This view relies on the widespread occurrence of Noachian Fe/Mg clay minerals interpreted as products of the alteration of preexisting silicates by (sub)surface liquid water (Bibring *et al.,* 2006; Ehlmann *et al.,* 2011; Carter *et al.,* 2013; Sun and Milliken, 2015; Viennet *et al.,* 2019). However, this may not be the entire story. In fact, some clay minerals can directly precipitate from magmatic fluids (Meunier *et al.,* 2008, 2012; Berger *et al.,* 2014, 2018; Viennet *et al.,* 2020). Because these minerals cannot be used as a proxy for the past presence of liquid water, it seems *a priori* difficult to consider such magmatic clay minerals as indicators of habitability. Still, as discussed here, magmatic clay minerals may offer fantastic opportunities for prebiotic reactions.

To date, the only occurrence of martian magmatic Fe/Mg clay minerals has been found in the evolved (alkali/felsic) mesostasis of Nakhla (Viennet *et al.,* 2020), the martian meteorite eponym for nakhlites. Whether these minerals are more than anecdotal on Mars is difficult to determine, especially given the fierce debate over the exact fraction of the martian crust made up of evolved (alkali/felsic) rocks (Sautter *et al.,* 2016; Udry *et al.,* 2018; Bouley *et al.,* 2020). Here, we report the presence of magmatic Fe/Mg clay minerals within the mesostasis of NWA 5790, an unaltered Amazonian nakhlite ($\sim$1.3–1.4 Ga; Nyquist *et al.,* 2001). In contrast to that of Nakhla, the mesostasis of NWA 5790 does not exhibit a high level of igneous differentiation, which makes this meteorite more archetypal of the martian crust (Udry *et al.,* 2018).

2. Materials and Methods

2.1. Section of NWA 5790 investigated

The section of NWA 5790 investigated here is the section B described in the work of Jambon *et al.* (2016). This section was selected because it does not exhibit any trace of terrestrial alteration (Jambon *et al.,* 2016) or ''desert varnish'' or ''caliche,'' that is, clay mineral sheets or calcite

[1]Muséum National d'Histoire Naturelle, Institut de Minéralogie, Physique des Matériaux et Cosmochimie, CNRS UMR 7590, Sorbonne Université, CNRS, Paris, France.
[2]Université Lille, CNRS, INRA, ENSCL, UMR 8207 - UMET - Unité Matériaux et Transformations, Lille, France.
[3]Centre National de la Recherche Scientifique (CNRS), Université de Poitiers, UMR 7285 IC2MP-Hydrasa, Poitiers, France.

veins produced by alteration (Tomkinson *et al.,* 2015; Balta *et al.,* 2017). The augite and olivine grains of the section investigated do not display any iddingsite, amphibole, or smectite vein (see Supplementary Fig. S1).

2.2. Scanning and transmission electron microscopy

Scanning electron microscopy and energy-dispersive X-ray spectroscopy (EDXS) mapping were performed on a thin section of Nakhla with a SEM-FEG Ultra 55 Zeiss (IMPMC, Paris, France) microscope operating at a 15 kV accelerating voltage and a working distance of 7.5 mm for imaging with backscattered electrons and EDXS mapping. Transmission electron microscopy in scanning mode (STEM) was performed on focused ion beam foils with a Thermo Fisher Titan Themis 300 microscope operated at 300 keV (CCM, Lille, France). Transmission electron microscopy–based hyperspectral EDXS data (see below) were obtained by using the super-X detector system that comprises four windowless silicon drift detectors of high sensitivity. The probe current was set at maximum 200 pA with a dwell time at 10 µs per pixel.

2.3. Focused ion beam preparations

Focused ion beam (FIB) ultrathin sections were extracted with an FEI Strata DB 235 (IEMN, Lille, France). Milling at low Ga-ion currents minimizes common artifacts, including local gallium implantation, mixing of components, creation of vacancies or interstitials, creation of amorphous layers, local compositional changes, or redeposition of the sputtered material on the sample surface (Wirth, 2009).

2.4. EDXS data processing

A key aspect of this work is the postprocessing of the collected EDXS hyperspectral data, performed by using the Hyperspy Python-based package (de La Pena *et al.,* 2017). The signal was first denoized by using PCA and then fitted by a series of Gaussian functions. The integrated intensities of the Gaussian functions were used to quantify the spectra with the Cliff-Lorimer method, using experimentally determined k-factors. Special care was taken to correct for absorption effect within the sample, in particular for oxygen X-rays. Absorption correction depends on thickness density, which can be determined by comparing quantification made by Iron L-lines and Iron K-lines (Morris, 1980). Each pixel was quantified independently, and end-member phases were identified based on mixing diagrams.

2.5. Raman spectroscopy

Raman was performed by using a homemade time-resolved Raman spectrometer (Beyssac *et al.,* 2017). The laser is a nanosecond-pulsed DPSS laser operating at 532 nm with a 1.2 ns duration (FWHM) for the pulse, 10 to 2000 Hz repetition rate, and up to 1 mJ output energy per pulse. The laser was focused at the sample surface through a microscope objective (×20, numerical aperture 0.42), and the Raman signal was collected in the backscattering geometry. A Notch filter was used to cut the Rayleigh scattering. The signal was collected in an optical fiber and sent into a modified Czerny-Turner spectrometer manufactured by Princeton Instruments to be measured with a PIMAX4 ICCD camera manufactured by Princeton Instruments.

3. Results

Like the other nakhlites, NWA 5790 is an unaltered cumulate rock that exhibits large euhedral or subhedral crystals of augite set in a crystalline mesostasis (Figs. 1 and S1). Consistent with previous reports (Tomkinson *et al.,* 2015; Jambon *et al.,* 2016; Balta *et al.,* 2017), petrographic observations show that the mesostasis of NWA 5790 is made of Na/Ca-plagioclases and K-feldspars embedding skeletal Fe-rich Ti-oxides and Ti-rich magnetites that host ilmenite exsolutions (Fig. 1). In addition to augite grains, the investigated section contains an unaltered euhedral olivine (Fig. S1) and a zone of about the same size composed of fibrous minerals (Fig. 1). This zone exhibits a radial structure, with a central pore of about 200 µm in diameter, surrounded by Fe/Mg clay minerals intimately mixed with Fe-Si-Al-Ca nanograins, themselves surrounded by dendrites of maghemite and rather amorphous Fe-Si-Al-Ca materials in contact with augite grains and the mesostasis (Fig. 1 and Supplementary Materials). In contrast to the contact with augite grains, the transition with the mesostasis is not sharp; some Na/Ca plagioclases and skeletal equiaxed Fe-rich Ti oxides are distributed within the observed

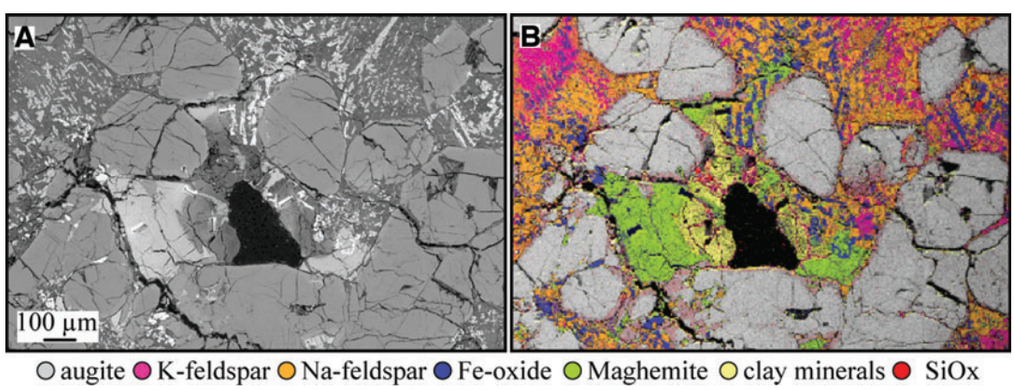

FIG. 1. Scanning electron microscope (SEM) image of the zone of NWA 5790 investigated in backscattered electron (BSE) mode (**A**) and the corresponding EDXS-based mineralogical map (**B**). Note the euhedral augite grains with no dissolution features surrounding the dendritic maghemite and Fe/Mg clay minerals. Color images are available online.

dendrites. These dendrites display a nearly paraboloidal fingerlike shape with side branches, that is, a columnar dendritic texture with trunks of a few to hundreds of microns in length (Fig. 2), typical of sudden cooling or quenching conditions.

The Fe/Mg clay minerals consist of layers of a few hundreds of nanometers in length stacked over a few tens of nanometers, with layer to layer distances of ~11.8 Å, a typical structure of smectites (Fig. 3). These Fe/Mg clay minerals are chemically heterogeneous, with a mean chemical composition falling between nontronite, celadonite, and saponite (Fig. 3). Most importantly, the observed anticorrelation between Mg and Cl (Fig. 3) attests to the presence of Cl within the structure of these Fe/Mg clay minerals according to the Mg-Cl crystallographic avoidance principle (Bailey, 1984). This assemblage of Cl-rich Fe/Mg clay minerals is highly porous and exhibits a network of microcavities or pockets, from tens of nanometers to several hundreds of nanometers in diameter (Fig. 4).

4. Discussion

These Fe/Mg clay minerals were clearly not produced via the aqueous alteration of preexisting silicates. In fact, the section of NWA 5790 investigated here has been recognized to be unaltered (Tomkinson *et al.,* 2015; Jambon *et al.,* 2016), and the alteration of the Ti-rich and Al-rich mesostasis (mainly made of feldspars) would have produced Ti-rich and Al-rich secondary minerals (Meunier and Velde, 2004). In contrast, the clay minerals described here display a low Al content (4 wt %) and do not contain any Ti. The Fe and Mg contents of these clay minerals could be consistent with the alteration of augite, but none of the augite grains of NWA 5790 display alteration textures such as retreating surfaces or pitchlike features resulting from dissolution. No contact with the Fe/Mg clay minerals could be observed as well. Also, the high Cl content of these Fe/Mg clay minerals is similar to that of Cl-rich magmatic apatites, scapolites, and amphiboles found in other nakhlites (Sautter *et al.,* 2006; McCubbin *et al.,* 2013; Giesting and Filiberto, 2016) and that of the magmatic Fe/Mg clay minerals found in Nakhla (Viennet *et al.,* 2020).

The subhedral/euhedral nature of augite crystals is consistent with slow growth within a magmatic chamber (Treiman, 2005; Jambon *et al.,* 2016; Udry and Day, 2018) or within a chilled margin of a lava flow or sill (Tomkinson *et al.,* 2015). The crystallization and the accumulation of augite grains led to the entrapment of a residual liquid enriched in Cl, potentially as a result of contamination by an exogenous Cl-rich fluid (McCubbin *et al.,* 2013; Udry and Day, 2018). With decreasing temperature, the Na/Ca plagioclases and the K-feldspars crystallized together with the skeletal equiaxed Fe-Ti oxides and the skeletal Ti-magnetites, eventually leading to the exsolution of a Cl/Fe-rich brine (Fig. 1). Here, the screw dislocations at the

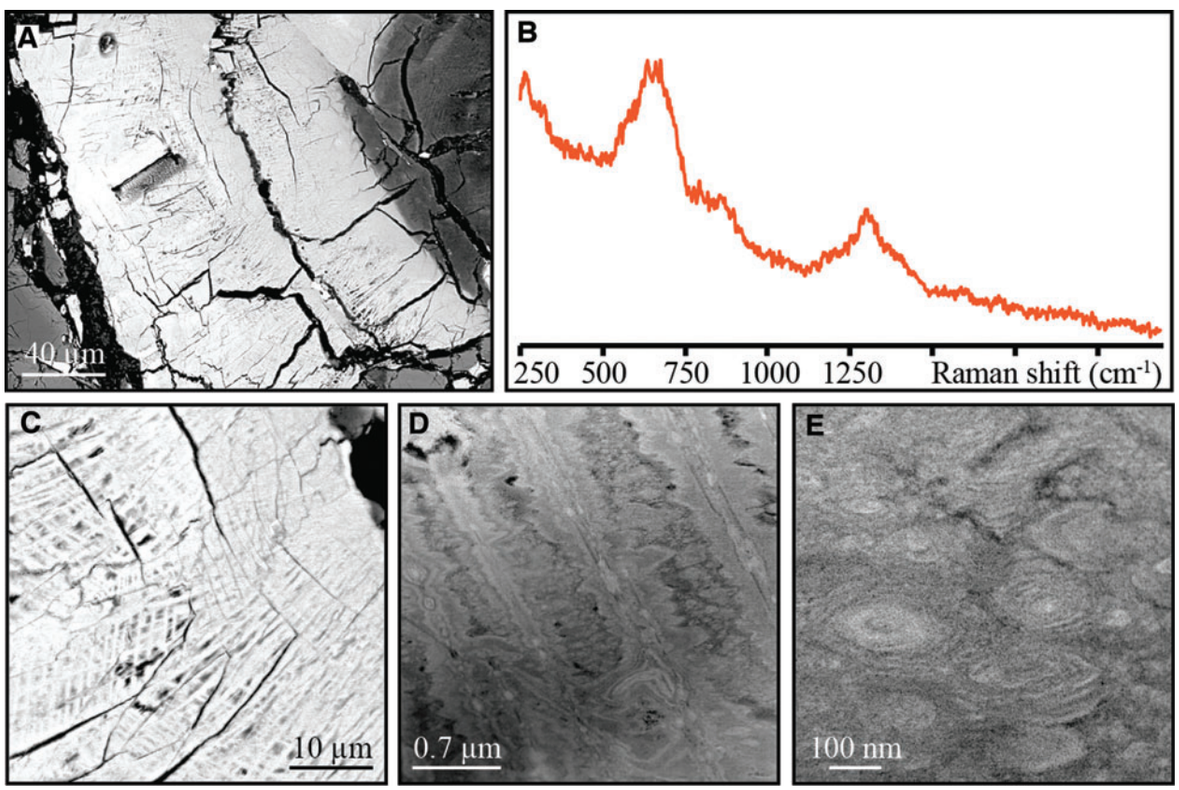

FIG. 2. Dendritic structures. (**A**) BSE image of the maghemite showing the location of the FIB foil shown in (D, E). (**B**) Time-resolved Raman spectra of the maghemite. (**C**) SEM image highlighting the dendritic texture of the maghemite. (**D**, **E**) Transmission electron microscope (TEM) images in STEM mode of the FIB section showing the screw shape of the dendritic texture along the main direction and the texture in spiral perpendicularly to the main direction. Color images are available online.

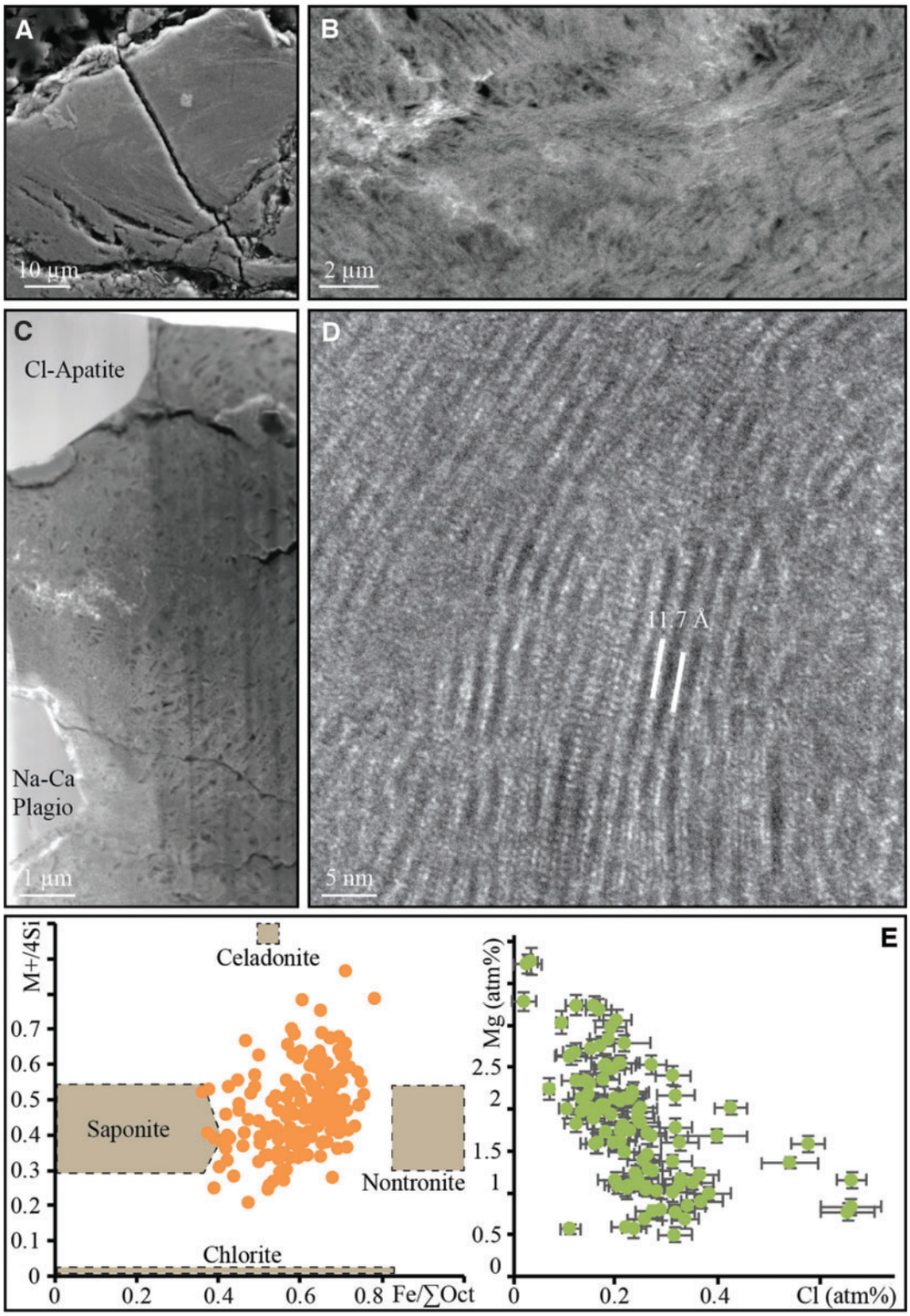

FIG. 3. Magmatic Fe/Mg clay minerals. (**A**) SEM image in BSE mode showing the huge mass of clay minerals. (**B**). SEM image in BSE mode showing the fibrous texture of the clay minerals. (**C**) TEM image in STEM mode of the FIB section (location shown in Fig. S2) showing the contact between Fe/Mg clay minerals and non-altered silicates. (**D**) TEM image in bright field showing the classical structure in sheets of the Fe/Mg clay minerals with a d-spacing of 11.7 Å. (**E**) Diagram showing the chemical composition of the Fe/Mg clay minerals and indicating a mixture of nontronite, celadonite and saponite (left) and plot showing the Mg content as a function of Cl content (right). Color images are available online.

AST-2020-2345-ver9-Viennet_1P.3d 02/24/21 8:52pm Page 5

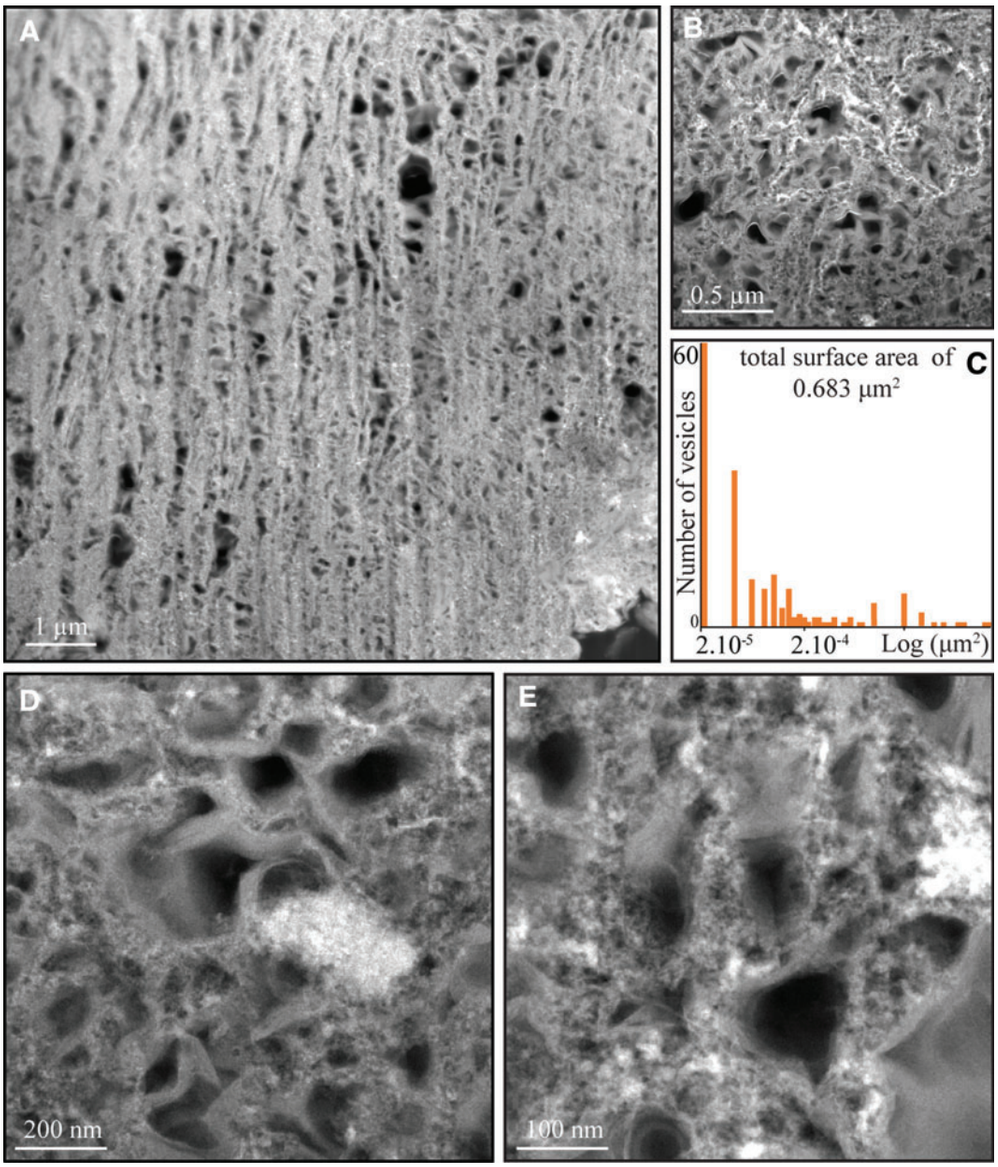

AU4 ▶ **FIG. 4.** Magmatic Fe/Mg clay minerals. (**A**) TEM image in STEM mode showing the vesicles formed by the Fe/Mg clay minerals. (**B**) Size distribution of the vesicles corresponding to the TEM images in STEM mode (E). (**C**–**E**). TEM images in STEM mode showing the vesicles formed by the Fe/Mg clay minerals. Color images are available online.

surface of the augite grains (together with the decrease of solubility of Fe III with decreasing temperature) potentially controlled the very fast precipitation of the observed dendrites, which explains their screw shapes and unidirectional solidification structures (Vernon, 2004). Masses of highly porous Cl-bearing Fe/Mg clay minerals then precipitated from the residual brine (together with, or right before, the Fe-Si-Al-Ca nanograins), that is, before reaching a high level of igneous differentiation in contrast to what occurred in Nakhla (Viennet *et al.,* 2020).

The magmatic production of Fe/Mg clay minerals evidenced here in a martian meteorite archetypal of the martian crust portends that a possibly significant fraction of the Fe/Mg clay minerals detected on Mars so far may not be the products of the aqueous alteration of preexisting silicates by (sub)surface water, questioning *a priori* the past habitability of Mars. Yet the magmatic Fe/Mg clay minerals described here have chemical and physical properties that offer fantastic opportunities for (prebiotic) organic reactions (Russell and Martin, 2004; Duval *et al.,* 2020). In fact, in addition to enabling electron transfer, their high Fe content may promote the synthesis and breakdown of universal metabolic precursors (Stucki, 2006), while their high Mg content may prompt both ribozyme-catalyzed and non-enzymatic RNA copying reactions (Adamala and Szostak, 2013).

Clay minerals have long been suggested as the perfect means of concentrating organic molecules onto their external surfaces and within their interlayer space so as to

AST-2020-2345-ver9-Viennet_1P.3d 02/24/21 8:52pm Page 6

be available for prebiotic reactions (Bernal, 1951; Ferris and Ertem, 1992; Brack, 2013; Lagaly *et al.,* 2013; Theng, 2018). The surface areas of the magmatic Fe/Mg clay minerals described here are very high; external and internal surface areas reach 30 μm^2 and 670 μm^2 per μm^3, respectively (*cf.* Supplementary Materials). For smectites, this corresponds to 2.4×10^{14} external sites and 5.8×10^{14} internal sites of possible interactions with organic functional groups (*cf.* Supplementary Materials).

Most importantly, the vesicular texture of these magmatic Fe/Mg clay minerals forms a network of chemically heterogeneous microcavities or pockets that offer even more optimal conditions for (prebiotic) organic reactions. In fact, most scenarios of the origin of life require boundaries or membranes (either organic or inorganic) to isolate, concentrate, and protect organic compounds that could eventually interact or react with each other (Szostak *et al.,* 2001; Hanczyc, 2003; Chen and Walde, 2010; Sun *et al.,* 2016). Plus, a boundary is a privileged interface for the formation of gradients that can promote organic reactions and be exploited as an energetic source (Monnard and Walde, 2015; Branscomb *et al.,* 2017; Branscomb and Russell, 2019). Here, more than 600 microcavities or pockets can be counted per μm^2 of clay minerals, with surfaces ranging from 1×10^{-5} to 1.4×10^{-2} μm^2 (Fig. 4C), each of them potentially a distinct microreactor for organic chemistry. The multiple connections between these microcavities or pockets may allow organic molecules to diffuse freely into, or out of, these microsystems, possibly leading to molecular crowding and, thereby, increasing the probability of achieving prebiotic chemical reactions.

AU2 ►

5. Conclusion

The section of the martian nakhlite NWA 5790 investigated here contains a zone composed of magmatic Fe/Mg clay minerals mixed with Fe-Si-Al-Ca nanograins surrounded by dendritic maghemite. These magmatic Fe/Mg clay minerals exhibit a vesicular texture that forms a network of microcavities or pockets that could serve as microreactors for the emergence of life. The fact that the formation of such niches for emerging life can be achieved via the magmatic precipitation of Fe/Mg clay minerals should make these aggregates a focus for research into the origin of life, especially as such magmatic Fe/Mg clay minerals form within liquid-water-poor environments (prebiotic reactions are thermodynamically out of equilibrium in aqueous solution; Lambert, 2008). *In fine,* by evidencing the formation of niches for emerging life on Mars even during the Amazonian, the present study provides a strong rationale for the possible emergence of life on other planetary bodies, including rocky and/or icy ones (such as Ceres, Enceladus, or Europa) on which the production of clay minerals has recently been reported (Waite *et al.,* 2017; Marchi *et al.,* 2019).

Acknowledgments

We thank Elisabeth Malassis for administrative simplification, the Atelier and the Cellule Projet (IMPMC) for the construction of the time-resolved Raman instrument @ IMPMC, David Troadec (IEMN) for the extraction of FIB foils, Imène Esteve (IMPMC) for her expert support with the SEM @ IMPMC, and Jean Michel Guigner (IMPMC) for his expert support with the TEM @ IMPMC. The authors would like to thank the collection of the Muséum National d'Histoire Naturelle for sharing the section of NWA 5790. The authors wish to acknowledge the Editor Dr. S.L. Cady, the associate editor C. McKay, as well as two anonymous reviewers for their constructive comments that greatly improved the quality of this work.

Author Contributions

J.C.V. and S.B. designed the present study. J.C.V. and S.B. conducted the SEM experiments. J.C.V. and O.B. conducted the Raman experiments. J.C.V., S.B., and C.L.G. conducted the TEM experiments. J.C.V. and C.L.G. performed SEM and TEM data reduction. All authors contributed to the interpretation of the results. J.C.V. and S.B. wrote the manuscript, with critical input from all authors.

Author Disclosure Statement

No competing financial interests exist.

Funding Information

The SEM facility @ IMPMC is supported by Region Ile de France grant SESAME Number I-07-593/R, INSU-CNRS, INP-CNRS and UPMC-Paris 6, and by the Agence Nationale de la Recherche (ANR) grant number ANR-07-BLAN-0124-01. The TEM facility @ Lille University is supported by the Chevreul Institute, the European FEDER and Région Nord-Pas-de-Calais.

References

Adamala, K., and Szostak, J.W. (2013) Nonenzymatic template-directed RNA synthesis inside model protocells. *Science* 342: 1098–1100.

Bailey, S.W., editor. (1984) *Micas,* De Gruyter, Boston.

Balta, J.B., Sanborn, M.E., Mayne, R.G., Wadhwa, M., McSween, H.Y., and Crossley, S.D. (2017) Northwest Africa 5790: a previously unsampled portion of the upper part of the nakhlite pile. *Meteorit Planet Sci* 52:36–59.

Berger, G., Meunier, A., and Beaufort, D. (2014) Clay mineral formation on Mars: chemical constraints and possible contribution of basalt out-gassing. *Planetary Geology Field Symposium, Kitakyushu, Japan, 2011: Planetary Geology and Terrestrial Analogs* 95:25–32.

Berger, G., Beaufort, D., and Antoine, R. (2018) Clay minerals related to the late magmatic activity of the Piton des Neiges (Réunion Island): consequence for the primitive crusts. *Clay Miner* 53:675–690.

Bernal, J.D. (1951) *The Physical Basis of Life,* Routledge and Paul, London.

Beyssac, O., Gauthier, M., Fau, A., Bernard, S., Benzerara, K., Morand, M., Rosier, P., Meslin, P.-Y., Maurice, S., SuperCam Science Team. (2017) Nanosecond time-resolved Raman and fluorescence spectroscopy: insights for mineral and organics characterization [abstract 1545]. In *48th Lunar and Planetary Science Conference,* Lunar and Planetary Institute, Houston.

Bibring, J.-P., Langevin, Y., Mustard, J.F., Poulet, F., Arvidson, R., Gendrin, A., Gondet, B., Mangold, N., Pinet, P., Forget, F., OMEGA Team. (2006) Global mineralogical and aqueous Mars history derived from OMEGA/Mars Express data. *Science* 312:400–404.

AST-2020-2345-ver9-Viennet_1P.3d 02/24/21 8:52pm Page 7

Bouley, S., Tuttle Keane, J., Baratoux, D., Langlais, B., Matsuyama, I., Costard, F., Hewins, R., Payré, V., Sautter, V., Séjourné, A., *et al.* (2020) A thick crustal block revealed by reconstructions of early Mars highlands. *Nat Geosci* 13:105–109.

Brack, A. (2013) Clay minerals and the origin of life. In *Developments in Clay Science,* Elsevier, Amsterdam, pp 507–521.

Branscomb, E., and Russell, M.J. (2019) Why the submarine alkaline vent is the most reasonable explanation for the emergence of life. *BioEssays* 41, doi:10.1002/bies.201800208.

Branscomb, E., Biancalani, T., Goldenfeld, N., and Russell, M. (2017) Escapement mechanisms and the conversion of disequilibria; the engines of creation. *Phys Rep* 677:1–60.

Carter, J., Poulet, F., Bibring, J.-P., Mangold, N., and Murchie, S. (2013) Hydrous minerals on Mars as seen by the CRISM and OMEGA imaging spectrometers: updated global view. *J Geophys Res Planets* 118:831–858.

Chen, I.A., and Walde, P. (2010) From self-assembled vesicles to protocells. *Cold Spring Harb Perspect Biol* 2, doi:10.1101/cshperspect.a002170.

de La Pena, F., Ostasevicius, T., Fauske, V.T., Burdet, P., Jokubauskas, P., Nord, M,. Sarahan, M., Prestat, E., Johnstone, D.N., Taillon, J., *et al.* (2017) Electron microscopy (big and small) data analysis with the Open Source software package HyperSpy. *Microsc Microanal* 23:214–215.

Duval, S., Branscomb, E., Trolard, F., Bourrié, G., Grauby, O., Heresanu, V., Schoepp-Cothenet, B., Zuchan, K., Russell, M.J., and Nitschke, W. (2020) On the why's and how's of clay minerals' importance in life's emergence. *Appl Clay Sci* 195, doi:10.1016/j.clay.2020.105737.

Ehlmann, B.L., Mustard, J.F., Murchie, S.L., Bibring, J.-P., Meunier, A., Fraeman, A.A., and Langevin, Y. (2011) Subsurface water and clay mineral formation during the early history of Mars. *Nature* 479:53–60.

Ferris, J., and Ertem, G. (1992) Oligomerization of ribonucleotides on montmorillonite: reaction of the 5'-phosphorimidazolide of adenosine. *Science* 257:1387–1389.

Giesting, P.A., and Filiberto, J. (2016) The formation environment of potassic-chloro-hastingsite in the nakhlites MIL 03346 and pairs and NWA 5790: insights from terrestrial chloro-amphibole. *Meteorit Planet Sci* 51:2127–2153.

Grotzinger, J.P., Sumner, D.Y., Kah, L.C., Stack, K., Gupta, S., Edgar, L., Rubin, D., Lewis, K., Schieber, J., Mangold, N., *et al.;* MSL Science Team. (2014) A habitable fluvio-lacustrine environment at Yellowknife Bay, Gale Crater, Mars. Science 343, doi:10.1126/science.1242777.

Hanczyc, M.M. (2003) Experimental models of primitive cellular compartments: encapsulation, growth, and division. *Science* 302:618–622.

Hurowitz, J.A., Grotzinger, J.P., Fischer, W.W., McLennan, S.M., Milliken, R.W., Stein, N., Vasavada, A.R., Blake, D.F., Dehouck, E., Eigenbrode, J.L., *et al.* (2017) Redox stratification of an ancient lake in Gale Crater, Mars. *Science* 356, doi:10.1126/science.aah6849.

Jambon, A., Sautter, V., Barrat, J.-A., Gattacceca, J., Rochette, P., Boudouma, O., Badia, D., and Devouard, B. (2016) Northwest Africa 5790: revisiting nakhlite petrogenesis. *Geochim Cosmochim Acta* 190:191–212.

Kral, T.A., Birch, W., Lavender, L.E., and Virden, B.T. (2014) Potential use of highly insoluble carbonates as carbon sources by methanogens in the subsurface of Mars. *Planet Space Sci* 101:181–185.

Lagaly, G., Ogawa, M., and Dékány, I. (2013) Clay mineral–organic interactions. In *Developments in Clay Science,* edited by F. Bergaya and G. Lagaly, Elsevier, Amsterdam, pp 435–505.

Lambert, J.-F. (2008) Adsorption and polymerization of amino acids on mineral surfaces: a review. *Orig Life Evol Biosph* 38:211–242.

Marchi, S., Raponi, A., Prettyman, T.H., De Sanctis, M.C., Castillo-Rogez, J., Raymond, C.A., Ammannito, E., Bowling, T., Ciarniello, M., Kaplan, H., *et al.* (2019) An aqueously altered carbon-rich Ceres. *Nat Astron* 3, doi:10.1038/s41550-018-0656-0.

McCubbin, F.M., Elardo, S.M., Shearer, C.K., Smirnov, A., Hauri, E.H., and Draper, D.S. (2013) A petrogenetic model for the comagmatic origin of chassignites and nakhlites: inferences from chlorine-rich minerals, petrology, and geochemistry. *Meteorit Planet Sci* 48:819–853.

McMahon, S., Bosak, T., Grotzinger, J.P., Milliken, R.E., Summons, R.E., Daye, M., Newman, S.A., Fraeman, A., Williford, K.H., and Briggs, D.E.G. (2018) A field guide to finding fossils on Mars. *J Geophys Res Planets* 123:1012–1040.

Meunier, A., and Velde, B.D. (2004) *Illite: Origins, Evolution and Metamorphism,* Springer-Verlag, Berlin Heidelberg.

Meunier, A., Mas, A., Beaufort, D., Patrier, P., and Dudoignon, P. (2008) Clay minerals in basalt-hawaiite rocks from Mururoa Atoll (French Polynesia). II. Petrography and geochemistry. *Clays Clay Miner* 56:730–750.

Meunier, A., Petit, S., Ehlmann, B.L., Dudoignon, P., Westall, F., Mas, A., El Albani, A., and Ferrage, E. (2012) Magmatic precipitation as a possible origin of Noachian clays on Mars. *Nat Geosci* 5:739–743.

Monnard, P.-A., and Walde, P. (2015) Current ideas about prebiological compartmentalization. *Life* 5:1239–1263.

Morris, P.L. (1980) The correction of thin foil microanalysis data for X-ray absorption effects. In *Electron Microscopy and Analysis 1979,* The Institute of Physics, London, pp 413–416.

Nyquist, L.E., Bogard, D.D., Shih, C.-Y., Greshake, A., Stöffler, D., and Eugster, O. (2001) Ages and geologic histories of martian meteorites. In *Chronology and Evolution of Mars,* edited by R. Kallenbach, J. Geiss, and W.K. Hartmann, Springer, Dordrecht, the Netherlands, 105–164.

Russell, M.J., and Martin, W. (2004) The rocky roots of the acetyl-CoA pathway. *Trends Biochem Sci* 29:358–363.

Sautter, V., Jambon, A., and Boudouma, O. (2006) Cl-amphibole in the nakhlite MIL 03346: evidence for sediment contamination in a martian meteorite. *Earth Planet Sci Lett* 252:45–55.

Sautter, V., Toplis, M.J., Beck, P., Mangold, N., Wiens, R., Pinet, P., Cousin, A., Maurice, S., DeDeit, L., Hewins, R., *et al.* (2016) Magmatic complexity on early Mars as seen through a combination of orbital, *in situ* and meteorite data. *Lithos* 254:36–52.

Stucki, J.W. (2006) Properties and behaviour of iron in clay minerals. In *Developments in Clay Science,* Elsevier, Amsterdam, pp 423–475.

Sun, V.Z., and Milliken, R.E. (2015) Ancient and recent clay formation on Mars as revealed from a global survey of hydrous minerals in crater central peaks. *J Geophys Res Planets* 120:2293–2332.

Sun, S., Li, M., Dong, F., Wang, S., Tian, L., and Mann, S. (2016) Chemical signaling and functional activation in colloidosome-based protocells. *Small* 12:1920–1927.

AST-2020-2345-ver9-Viennet_1P.3d 02/24/21 8:52pm Page 8

Szostak, J.W., Bartel, D.P., and Luisi, P.L. (2001) Synthesizing life. *Nature* 409:387–390.

Theng, B.K.G. (2018) *Clay Mineral Catalysis of Organic Reactions,* CRC Press, Taylor & Francis Group, Boca Raton, FL.

Tomkinson, T., Lee, M.R., Mark, D.F., Dobson, K.J., and Franchi, I.A. (2015) The Northwest Africa (NWA) 5790 meteorite: a mesostasis-rich nakhlite with little or no martian aqueous alteration. *Meteorit Planet Sci* 50:287–304.

Treiman, A.H. (2005) The nakhlite meteorites: augite-rich igneous rocks from Mars. *Geochemistry* 65:203–270.

Udry, A., and Day, J.M.D. (2018) 1.34 billion-year-old magmatism on Mars evaluated from the co-genetic nakhlite and chassignite meteorites. *Geochim Cosmochim Acta* 238:292–315.

Udry, A., Gazel, E., and McSween, H.Y., Jr. (2018) Formation of evolved rocks at Gale Crater by crystal fractionation and implications for Mars crustal composition. *J Geophys Res Planets* 123:1525–1540.

Vernon, R.H. (2004) *A Practical Guide to Rock Microstructure,* Cambridge University Press, Cambridge, UK.

Viennet, J.-C., Bultel, B., and Werner, S.C. (2019) Experimental reproduction of the martian weathering profiles argues for a dense Noachian CO_2 atmosphere. *Chem Geol* 525: 82–95.

Viennet, J.-C., Bernard, S., Le Guillou, C., Sautter, V., Schmitt-Kopplin, P., Beyssac, O., Pont, S., Zanda, B., Hewins, R., and Remusat, L. (2020) Tardi-magmatic precipitation of martian Fe/Mg-rich clay minerals via igneous differentiation. *Geochemical Perspectives Letters* 14:47–52.

Waite, J.H., Glein, C.R., Perryman, R.S., Teolis, B.D., Magee, B.A., Miller, G., Grimes, J., Perry, M.E., Miller, K.E., Bouquet, A., *et al.* (2017) Cassini finds molecular hydrogen in the Enceladus plume: Evidence for hydrothermal processes. *Science* 356, 155–159.

Westall, F., Loizeau, D., Foucher, F., Bost, N., Betrand, M., Vago, J., and Kminek, G. (2013) Habitability on Mars from a microbial point of view. *Astrobiology* 13:887–897.

Wirth, R. (2009) Focused ion beam (FIB) combined with SEM and TEM: advanced analytical tools for studies of chemical composition, microstructure and crystal structure in geomaterials on a nanometre scale. *Chem Geol* 261:217–229.

Address correspondence to:
Jean-Christophe Viennet
Muséum National d'Histoire Naturelle
Institut de Minéralogie, Physique
des Matériaux et Cosmochimie
CNRS UMR 7590
Sorbonne Université, CNRS
F-75005 Paris
France

E-mail: jean.christophe.viennet25@gmail.com

Submitted 28 July 2020
Accepted 22 December 2020
Associate Editor: Christopher McKay

Abbreviations Used

BSE = backscattered electron
EDXS = energy-dispersive X-ray spectroscopy
FIB = focused ion beam
SEM = scanning electron microscope
STEM = scanning transmission electron microscopy
TEM = transmission electron microscope

AUTHOR QUERY FOR AST-2020-2345-VER9-VIENNET_1P

AU1: I defined EDXS here and in the abbreviations list. OK?
AU2: I replaced the dots with multiplication x's. OK?
AU3: I defined BSE here and in the abbreviations list. OK?
AU4: Please confirm the descriptions of panels B and C, compared to the figure.